# Effect of silicic acid on arsenate and arsenite retention mechanisms on 6-L ferrihydrite: A spectroscopic and batch adsorption approach

**Xiaodong Gao**[a,†], **Robert A. Root**[a], **James Farrell**[b], **Wendell Ela**[b], and **Jon Chorover**[a,*]

[a]Department of Soil, Water and Environmental Science, University of Arizona, Tucson, AZ 85721

[b]Department of Chemical and Environmental Engineering, University of Arizona, Tucson, AZ 85721

## Abstract

The competitive adsorption of arsenate and arsenite with silicic acid at the ferrihydrite-water interface was investigated over a wide pH range using batch sorption experiments, attenuated total reflectance Fourier transform infrared (ATR-FTIR) spectroscopy, extended X-ray absorption fine structure (EXAFS) spectroscopy, and density functional theory (DFT) modeling. Batch sorption results indicate that the adsorption of arsenate and arsenite on the 6-L ferrihydrite surface exhibits a strong pH-dependence, and the effect of pH on arsenic sorption differs between arsenate and arsenite. Arsenate adsorption decreases consistently with increasing pH; whereas arsenite adsorption initially increases with pH to a sorption maximum at pH 7–9, where after sorption decreases with further increases in pH. Results indicate that competitive adsorption between silicic acid and arsenate is negligible under the experimental conditions; whereas strong competitive adsorption was observed between silicic acid and arsenite, particularly at low and high pH. In-situ, flow-through ATR-FTIR data reveal that in the absence of silicic acid, arsenate forms inner-sphere, *binuclear bidentate*, complexes at the ferrihydrite surface across the entire pH range. Silicic acid also forms inner-sphere complexes at ferrihydrite surfaces throughout the entire pH range probed by this study (pH 2.8 – 9.0). The ATR-FTIR data also reveal that silicic acid undergoes polymerization at the ferrihydrite surface under the environmentally-relevant concentrations studied (e.g., 1.0 mM). According to ATR-FTIR data, arsenate complexation mode was not affected by the presence of silicic acid. EXAFS analyses and DFT modeling confirmed that arsenate tetrahedra were bonded to Fe metal centers via binuclear bidentate complexation with average As(V)-Fe bond distance of 3.27 Å. The EXAFS data indicate that arsenite forms both mononuclear bidentate and binuclear bidentate complexes with 6-L ferrihydrite as indicated by two As(III)-Fe bond distances of ~2.92–2.94 and 3.41–3.44 Å, respectively. The As-Fe bond distances in both arsenate and arsenite EXAFS spectra remained unchanged in the presence of Si, suggesting that whereas Si diminishes arsenite adsorption preferentially, it has a negligible effect on As-Fe bonding mechanisms.

[*]corresponding author: Jon Chorover, The University of Arizona, chorover@cals.arizona.edu, Telephone: 520-626-5635; Fax: 520-621-1647.

[†]Current address: Department of Earth Science, Rice University, Houston, TX 77251, xdgao@rice.edu

## 1. Introduction

Arsenic derived from natural or anthropogenic sources occurs widely in groundwater and surface water in many countries, posing a severe health threat to millions of people worldwide. It is a redox active element that occurs in the environment primarily in inorganic form and in one of two oxidation states - As(V) and As(III) - which together likely represent > 99% of total arsenic in soils, sediments and waters (Ryu et al., 2002). Arsenate generally predominates in oxygenated waters, whereas arsenite can be prevalent in suboxic groundwater. The latter is considered more mobile and more toxic in natural environments. The aqueous environmental concentration of arsenic is governed largely by mineral-surface interactions. Adsorption or coprecipitation with metal oxides, particularly Fe (oxyhydr)oxides, is an important process controlling the fate and transport of arsenic in natural aquatic systems due to their abundance in the environment and high affinity for arsenic species. For this reason, hydrous ferric oxides, such as ferrihydrite, are routinely used as adsorbents to remove arsenic from the aqueous phase during engineered water and wastewater treatment (Mohan and Pittman, 2007).

The molecular-scale adsorption mechanisms of arsenate and arsenite on a range of natural and synthetic minerals (e.g., metal oxides, silicates) have been extensively investigated using macroscopic and spectroscopic techniques including synchrotron X-ray absorption and FTIR spectroscopies (Sun and Doner, 1996; Fendorf, et al., 1997; Raven et al., 1998; Goldberg and Johnston, 2001; Farquhar et al., 2002; Dixit and Hering, 2003). According to these studies, both arsenate and arsenite are strongly adsorbed on polyvalent metal (oxyhydr)oxide surfaces, forming predominantly inner-sphere surface complexes by ligand exchange reactions resulting in either monodentate or binuclear bidentate complexes depending on surface loading and solution chemistry. Only a few prior studies reported that arsenite forms both inner-sphere and outer-sphere surface complexes on ferric (oxyhydr)oxide surfaces (Goldberg and Johnston, 2001; Catalano et al., 2008).

It is well known that the presence of other naturally occurring anions in solution may compete for sorption sites on mineral surfaces and thereby affect the stability and mobility of adsorbed arsenic species. Previous research has indicated that individual anion species exhibit widely different affinities for mineral surface sites. For example, Goh and Lim (2005) reported that the capabilities of common anions to increase arsenic mobility in subsurface environments follow the order: phosphate > carbonate > sulfate ≈ chloride. Among these anions, phosphate is particularly effective at competing with arsenate for sorption sites due to their similarities in coordination geometry and geochemical behavior (Liu et al., 2001; Roberts et al., 2004; Goh and Lim, 2005; Impellitteri, 2005; Frau et al., 2008).

Silicic acid, present dominantly as the neutral $Si(OH)_4{}^0{}_{(aq)}$ species at pH < 9, is one of the principal inorganic ligands in soil and water systems, and it occurs at concentrations ranging from 5 – 35 mg $L^{-1}$ (0.17 – 1.24 mM) in natural soils and surface waters (Iller, 1979). Adsorption of silicic acid on Fe (oxyhydr)oxides has been studied previously (Waltham and Eick, 2002; Doelsch et al., 2003; Luxton et al., 2006; Swedlund et al., 2009, 2010). Similar to other naturally occurring ligands such as phosphate and sulfate, silicic acid can adsorb

strongly onto Fe oxyhydroxide surfaces via bidentate, inner-sphere surface complexes (Swedlund et al., 2009, 2010), suggesting that silicic acid might have a significant role in arsenic mobilization in both natural and engineered environments via competitive sorption for mineral surface sites. In addition, silicic acid can undergo surface-induced polymerization at or below environmentally-relevant concentrations (i.e., < 1.0 mM) (Swedlund et al., 2009; 2010), thereby altering the surface properties of the underlying substrate (e.g., metal oxides). As a result, adsorption mechanisms of silicic acid on metal oxides and their effects on arsenic adsorption are likely to vary significantly across environmentally-relevant Si concentration ranges. Despite the fact that silicic acid is one of the major ligands in natural waters and is often present at concentrations >10 times higher than phosphate, silicic acid has been less studied than other common ligands for its effects on arsenic adsorption in natural systems. A few macroscopic studies suggested that silica significantly diminished the adsorption of arsenite to Fe oxyhydroxides, whereas it has a negligible effect on arsenate adsorption (Waltham and Eick, 2002; Luxton et al., 2006). However, several other studies have reported that both arsenate and arsenite removal by ferric hydroxides was substantially decreased by the presence of silica (Meng et al., 2000; Davis et al., 2001). We hypothesized that elucidation of molecular-scale competitive adsorption mechanisms would help to resolve the discrepancy in the literature and to accurately predict the effect of silica on the stability and mobility of arsenic in engineered water treatment systems using hydrous ferric oxide as an adsorbent, as well as in groundwater and vadose zone solutions.

Therefore, the main objective of this study was to examine the effect of silicic acid on the extent and molecular mechanisms of both arsenate and arsenite adsorption to a model Fe(III) oxyhydroxide (ferrihydrite, $Fe_5HO_8{\bullet}4H_2O$). Ferrihydrite was chosen because it is commonly employed as an adsorbent for arsenic removal during drinking water treatment (Mohan and Pittman, 2007) and it is also one of the most common naturally occurring Fe oxyhydroxides that can precipitate from many types of ferriferous solutions at the Earth's surface (Yu et al., 1999). This poorly crystalline mineral phase often has high specific surface area and reactive hydroxyl group site density, both of which make it a high affinity adsorbent for trace metal(loid) contaminants (Raven et al., 1998; Dixit and Hering, 2003). The in-situ molecular spectroscopic techniques of attenuated reflectance-Fourier transform infrared (ATR-FTIR) and extended X-ray absorption fine structure (EXAFS) were combined with batch adsorption methods to elucidate the effect of silicic acid on arsenic adsorption mechanisms at ferrihydrite surfaces across a gradient in pH that is representative of natural waters. The results of the batch experiments and spectroscopic analyses were further analyzed using density functional theory (DFT) modeling to quantify the bond energies associated with the spectroscopic indications of surface speciation of As(III), As(V) and $Si(OH)_4$ and their complexation modes at ferrihydrite surfaces.

## 2. Material and method

### 2.1 Materials

**2.1.1 Arsenate and arsenite salts—**$Na_2HAsO_4{\bullet}7H_2O$ (≥ 98%) and $NaAsO_3$ (≥ 99%), were purchased from Sigma-Aldrich Co. (St. Louis, MO) and used as received. Silicic acid

($Si(OH)_4$) solution was prepared following the methods of Iler (1979) by mixing 1 g silica ($SiO_2$, 99.8%, Sigma-Aldrich) with 8.0 g of 50:50 (w/w) NaOH:$H_2O$ and 30 g of $H_2O$ on an end-over-end shaker (7 rpm) for 24 h. The solution was then diluted to 1 L with Barnstead Nanopure (NP) $H_2O$ (18.2 MΩ) to obtain 16.6 mM $Si(OH)_4$ solution, which was further diluted to ~1.66 mM, with pH adjusted from ~11.5 to 8.0 by dropwise addition of 0.1 M HCl to depolymerize silica. Desired concentration of arsenate or arsenite solutions (i.e., 0.1 and 1.0 mM) were freshly prepared before each experiment using NP water either in the absence or the presence of 1.0 mM $Si(OH)_{4(aq)}$.

**2.1.2 Six-line ferrihydrite synthesis and characterization—**Six-line ferrihydrite was synthesized using the method of Burleson and Penn (2006). Briefly, 250 mL of 0.48 M $NaHCO_3$ (99.9%, Mallinckrodt) was added to an equal volume of 0.4 M $Fe(NO_3)_3$•$9H_2O$ (JB Baker, 98.8%) using a peristaltic pump during vigorous stirring over 120 min. Once the addition of $NaHCO_3$ solution was complete, the suspension was microwave-annealed at 40 s intervals until it boiled to improve homogeneity of the nanoparticulate suspension. Immediately after heating, the suspension was plunged into an ice bath, brought to room temperature, and then transferred into dialysis tubing (Spectra/Por 7, 1000 MWCO) and dialyzed against NP water at 4 °C for 3 d, with dialysis water changed three times per day. A portion of the ferrihydrite colloidal suspension was freeze-dried and gently ground using an agate mortar and pestle for characterization, analysis and batch adsorption experiments. The remainder of the suspension was transferred to a polyethylene bottle and stored at 4 °C for spectroscopic studies. The ferrihydrite suspension was used within 3 weeks from synthesis in the experiments.

The X-ray diffraction (XRD) pattern of the synthetic material collected at Stanford Synchrotron Radiation Lightsource (SSRL) on beamline 11-3 shows 6 broad peaks, indicating its poor crystallinity (see Figure S1). Peak positions and intensities are in good agreement with the XRD pattern for 6-line ferrihydrite (Schwertmann and Cornell, 1991). Specific surface area was calculated in accordance with BET theory using $N_2$ adsorption data obtained at 77 K on a Beckman Coulter SA 3100 Gas Adsorption Surface Area Analyzer (Beckman Coulter Inc., Fullerton, CA). The result indicated that the synthetic 6-L ferrihydrite had a specific surface area of 311 ± 1.2 $m^2\ g^{-1}$.

## 2.2 Batch adsorption experiments

Batch As(V) adsorption envelopes were collected as a function of pH (3.0–10.0) in duplicate at 25 ºC with initial As concentrations of 0.1 and 1.0 mM with or without 1.0 mM $Si(OH)_{4(aq)}$. Solutions of 100 mM HCl or NaOH were used to adjust the suspension pH to achieve a final pH range of 3.0 – 10.0. For each replicate in the sorption experiment, 75 mg freeze-dried ferrihydrite were added to a 35 mL polyethylene centrifuge tube before 15 mL of arsenate (with or without $Si(OH)_4$) solution were introduced. A separate set of experiments were conducted with Si alone (no As) for direct comparison. The final solid concentration of ferrihydrite in the reaction suspension was 5.0 g $L^{-1}$. Suspensions were equilibrated on an end-over-end shaker (7 rpm) for 24 h. This period of time was sufficient to reach sorption equilibrium (no further uptake) based on preliminary experiments. The pH of each suspension was checked and adjusted every 1 h until it stabilized at target values

during the reaction. Adsorbent-free controls (no ferrihydrite) were reacted concurrently to monitor for unintended compound loss to vessel surfaces. At the end of batch sorption experiments, the equilibrium suspensions were centrifuged at 12,812 *g* and 25 °C for 30 min. The supernatant was aspirated and filtered through a 0.2 μm nominal pore size syringe filter. An aliquot of the filtrate was acidified to pH < 2.0 with 1% trace metal grade $HNO_3$ and analyzed for total As, Si and Fe concentrations using a Perkin-Elmer Elan DRC II inductively coupled plasma-mass spectrometer (ICP-MS). The amount of adsorbed As(V) was calculated on the basis of loss from solution corrected for adsorbent free blank losses (undetectable). The wet pastes from centrifugation were immediately frozen prior to As speciation analysis using arsenic-XANES and EXAFS spectroscopy at Stanford Synchrotron Radiation Lightsource (SSRL).

Batch adsorption for As(III) on 6-L ferrihydrite were performed as described above for As(V) but with the following modifications. Since previous studies reported that arsenite associated with Fe and Mn oxyhydroxides in aqueous systems can be oxidized to arsenate by photolytically produced free radicals (Bednar et al., 2002), specific precautions were employed to prevent this reaction. All polyethylene centrifuge tubes containing sorbent suspensions were immediately flushed with $N_2$ gas and sealed to prevent atmospheric exposure, and all were wrapped in aluminum foil to prevent photochemical oxidation during the adsorption experiments. The samples were equilibrated, centrifuged, and filtered as described above. Immediately after filtration, 100 μL of 0.15 M ethylenediaminetetraacetic acid (EDTA) solution was spiked into the filtrate as a preservative to stabilize As speciation (Bednar et al., 2002). An aliquot of the preserved filtrate was analyzed for total As, Si and Fe concentrations using ICP-MS within 24 h from the batch experiment. In addition, aqueous As speciation analysis was performed to confirm the efficacy of the preservation techniques using an HPLC equipped with an anion exchange column to separate the arsenic species prior to on-line injection to ICP-MS. Prior to the speciation analysis, the preserved filtrate was diluted with 50 mM $(NH_4)_2CO_3$ (HPLC mobile phase). Wet pastes were kept frozen before As solid-state speciation analysis using As-XANES and EXAFS spectroscopy at the Stanford Synchrotron Radiation Lightsource (SSRL).

### 2.3 Flow-through ATR-FTIR spectroscopy experiments

In-situ ATR-FTIR spectroscopy is a surface-sensitive technique that can be used to interrogate molecular-scale interactions that occur at the adsorbent-solution interface. ATR-FTIR spectra were obtained using a Magna-IR 560 Nicolet spectrometer (Madison, WI) equipped with purge gas generator and a deuterated triglycine sulfate (DTGS) detector. Although arsenite does not exhibit distinct bands in the mid-IR spectral range (4000 – 600 $cm^{-1}$) at pH < 9.0 (Goldberg and Johnston, 2001), competitive adsorption between arsenate and silicic acid was nonetheless susceptible to probing with ATR-FTIR spectroscopy. A 45° trapezoidal germanium (Ge) internal reflection element (IRE) (56 × 10 × 3 mm) was employed within a flow-through ATR cell (Pike Technologies). The Ge IRE in the flow cell was coated with a thin layer of 6-L ferrihydrite by evenly depositing 500 μL nanoparticulate ferrihydrite suspension on the IRE surface. After drying overnight under vacuum, the coated Ge IRE was placed on a horizontal ATR sample stage inside the spectrometer. A new coating was prepared for each experiment, and spectra of dry films were collected to

determine the consistency of coating. The ATR cell was connected to a reaction vessel containing 1 L of either single metalloid (As or Si) solution or dual metalloid (As and Si) solution, continuously stirred with a magnetic bar. A peristaltic pump was used to deliver the solution from the reaction vessel through the flow cell at a constant flow rate of 0.5 mL $min^{-1}$. The ATR-FTIR adsorption experiments were conducted only at the higher arsenic and silica concentration (i.e., 1 mM) due to the high detection limit of the ATR-FTIR technique.

All spectra were acquired at room temperature with 4.0 $cm^{-1}$ resolution with 400 scans over the spectral range of 4000 – 600 $cm^{-1}$ using the autogain function and aperture set at 100. For each experiment, background solution (i.e., 1 mM NaCl) was first pumped through the ATR cell, allowing the ferrihydrite coating to equilibrate at a given pH. The final background spectrum was collected when no further changes in the spectra were observed. Then, 1.0 mM arsenic solution in the absence or presence of 1.0 mM $Si(OH)_4$ was injected into the cell to initiate the adsorption experiment. Spectra were collected as a function of pH (3.0 – 10.0) and reaction time at 15 min intervals until adsorption equilibrium was reached as indicated by no furthers changes between successive spectra. The pH of the solution in the reaction vessel was monitored throughout the measurement, and adjusted as necessary by addition of 10 mM NaOH or HCl. A final sample spectrum was obtained by subtracting the appropriate background spectrum (e.g., 1.0 mM NaCl, 1.0 mM $Si(OH)_4$) from the sample spectrum. All data collection and spectral processing, including background subtraction and baseline correction, were performed using the OMNIC program (Thermo Nicolet, Co.).

### 2.4 Extended X-ray absorption fine structure spectroscopy measurements

Wet paste samples from batch adsorption experiments were transported frozen to SSRL and prepared for interrogation in an inert atmosphere ($N_2$ glove box). Briefly, 100–200 mg of the wet paste sample were loaded in a Teflon sample holder, sealed with Kapton tape, and kept in the glove box until data collection. Arsenic K-edge EXAFS spectra were collected for samples with an initial As concentration of 1.0 mM in the absence or presence of 1.0 mM Si at pH 3.0, 6.0, and 9.0 for arsenite and 3.0 and 9.0 for arsenate, respectively. Spectra were collected at SSRL beamline 4-1 or 11-2 using a Si (220) monochromator crystal with samples held in a liquid He cryostat using both fluorescence and transmission mode for a minimum of five scans for each sample. The two beamlines 4-1 and 11-2 have 13-element and 30-element Ge fluorescence detectors, respectively.

XAS data reduction and analyses were performed using SIXPACK software package (Webb, 2006) and EXAFSPAK (George and Pickering, 2000) as described elsewhere (Root et al., 2007). Briefly, fluorescence and transmission X-ray absorption spectra (EXAFS and XANES) were averaged using the SIXPACK software package and background subtracted and normalized to unity using the average post edge oscillation with PROCESS in EXAFSPAK. Isolation of backscattering contributions was accomplished by fitting a cubic spline function to the absorption envelope. The isolated function was then transformed from units of eV to $Å^{-1}$ to produce the EXAFS function ($\chi[k]$), where $k$ ($Å^{-1}$) is the photoelectron wave vector, which was then weighted by $k^3$ and fit by non-linear least-squares methods on

individual atomic shells in *k*-space using the entire *k*-range in the fit with the OPT program in EXAFSPAK (George and Pickering, 2000) (see O'Day et al., 2004a,b). Theoretical phase-shift and amplitude functions were calculated with the program FEFF (Rehr, 1993) using atomic clusters taken from the crystal structures of known As(III) and As(V) compounds with geometries similar to those expected in the unknown samples; specifically, angelellite for As(V) and schneiderhohnite for As(III). Multiple scattering from $As^{(V)}$-O tetrahedra was considered in the As(V) fits and was shown to improve the fit (Beaulieu and Savage, 2005; Ona-Nguema et al., 2005). Multiple scattering was not significant for As(III) because of static disorder in the ligating oxygen shell. Based on empirical fits to known arsenic and iron reference compounds, estimated errors were R ± 0.01 Å, N or $\sigma^2$ ± 15% for the first coordination shell, and R ± 0.02Å, N or $\sigma^2$ ± 30% for atoms beyond the first shell (see O'Day et al., 2004a,b). The oxidation state of arsenic was determined with XANES by fitting the normalized edge jump using linear least-squares combinations of reference compound spectra with the computer packages DATFIT (George and Pickering, 2000). Energy was allowed to vary in fits to account for small differences in energy calibration between samples and references. Shifts in energy of greater than 0.85 eV were rejected as spurious, which were well below the difference in edge peak position (>3 eV) between arsenite (11871 eV) and arsenate (11875 eV).

### 2.5 Molecular modeling of surface complexation

Density functional theory (DFT) is a quantum mechanical modeling method that has previously been employed to describe arsenic adsorption on ferric hydroxides (Zhang et al., 2005). DFT simulations were performed to determine the binding energies for As(V), As(III) and $Si(OH)_4$ species to ferric hydroxides. Ferric hydroxides were simulated using clusters similar to those used in several previous studies (Sherman and Randall, 2003; Zhang et al., 2005; Kubicki et al., 2007). As illustrated in Figure S2 (see supporting information), the clusters consisted of two Fe atoms in octahedral coordination with 10 O atoms, with the general formula $Fe_2O_3(H_2O)_7$. Clusters with different numbers of hydrogen atoms were also used in order to simulate binding sites with positive or negative charges. The speciation of the surface binding sites as a function of pH is shown in Figure S3.

DFT calculations were performed using the $DMol^3$ (Delley, 1990; 2000) package in the Accelrys Materials Studio modeling suite (Accelrys Corp., San Diego, CA ) on a personal computer. All calculations used double-numeric with polarization (DNP) basis sets (Delley, 1996), the gradient corrected VWN-BP functional for exchange and correlation, and included all electrons with unrestricted spins. Implicit solvation was incorporated into all aqueous phase simulations using the COSMO-ibs (Delley, 2006) solvation model. As recommended by previous investigators, the simulations also included one explicit water molecule in order to allow for hydrogen bonding and better outlying charge correction for negatively charged species (Kelly et al., 2006).

The geometry of the binding sites was optimized without any geometry constraints. In order to simulate the binding sites being part of a larger ferric hydroxide structure, simulations that included bound arsenic species employed geometry constraints that fixed the positions of oxygen atoms that were not part of the binding reaction. This was necessary in order to

avoid gross distortions of the dioctahedral geometry seen in previous investigations performed using similar ferric hydroxide clusters (Kubicki et al., 2007). Frequency calculations were performed on structures without geometry constraints in order to determine zero-point vibration energies and thermal corrections.

Gibbs free energy changes for complexation of As(V), As(III) and $Si(OH)_4$ with the binding site were calculated using published literature values for the dissolved species and DFT calculated values for the complexes and binding sites. Standard Gibbs energies of formation ($\Delta G_f^0$) for the binding sites and arsenic complexes were determined from the DFT calculated formation energies ($\Delta G_f^{DFT}$) by adjusting the vacuum scale to the standard thermodynamic and electrochemical scales. For uncharged structures, the $\Delta G_f^{DFT}$ values were converted to $\Delta G_f^0$ by subtracting $\Delta G_f^{DFT}$ energies calculated for the elements in their natural state at 25° and 1 atm. Energies for charged structures were also adjusted to the electrochemical scale by adding 99.6 kcal/mol for the standard hydrogen electrode (SHE) reaction ( $\Delta G^\circ_{SHE}$) to the $\Delta G_f^{DFT}$ for all species with a −1 charge and subtracting $\Delta G^\circ_{SHE}$ for all species with a +1 charge.

Based on previous research investigating similar systems, the $\Delta G_f^0$ values calculated for the binding sites and surface complexes may be expected to be accurate to within ±5 kcal $mol^{-1}$ (Paul et al., 2006; Zhu et al., 2009). However, errors in calculating standard Gibbs free energies of reaction ($\Delta G_r^0$) may be smaller, since bias in the calculations would largely cancel because only differences in energy between similar structures are used to calculate these values. The standard Gibbs free energies of formation used in all calculations and the stoichiometry and Gibbs free energy changes for the binding reactions for As(V), As(III) and Si are listed in Tables S1–S4 in the supporting information. Given the ±5 kcal $mol^{-1}$ errors, using the $\Delta G_f^0$ to model competitive binding will not be as accurate as conventional surface complexation modeling where robust surface complexation constants have been developed.

## 3. Results and discussion

### 3.1 Quantitative batch adsorption measurements

**3.1.1 Silicic acid effects on arsenate adsorption to ferrihydrite—**Adsorption of arsenate to ferrihydrite was measured as a function of initial arsenate concentration (0.1 and 1.0 mM) and pH (3.0 to 11.0) for a 24 h reaction time. Arsenate shows strong affinity for ferrihydrite surfaces and adsorption exhibits no pH-dependence at pH < ~ 9.0 (Figure 1a), with nearly 100% removal from aqueous solution in the single ion system. At pH > 9, arsenate adsorption on ferrihydrite decreases consistently with increasing pH. This pH-dependent adsorption of arsenate on Fe (oxyhydr)oxides has been well documented and can be partially explained by the pH-dependence of ferrihydrite surface charge (Figure S3) and arsenate aqueous speciation. Arsenic acid ($H_3AsO_4$) is a strong triprotic acid with $pKa_{(1–3)}$ values of 2.20, 6.97, and 11.53 (Raven et al., 1998). At pH < point zero net proton charge ($pH_{pznpc}$) of ferrihydrite (*ca*. pH 9, Figure S3) the mineral surface exhibits a net positive charge and a higher affinity for the negative changed oxyanion arsenate species ($H_2AsO_4^-$ or $HAsO_4^{2-}$). However, with increasing pH, ferrihydrite surface hydroxyl groups undergo progressive deprotonation, with the surface becoming net negatively charged at pH >

$pH_{pznpc}$. This results in an electrostatic repulsive force between the two negatively charged species ($HAsO_4^{2-}$ and $\equiv$Fe-$O^-$). The pH-dependent adsorption trend is similar for the two arsenate concentrations, except that the adsorption envelope decreases more steeply for 1.0 mM relative to 0.1 mM initial arsenate concentration (Figure 1a). Despite like-charge repulsion, substantial adsorption persists at pH > $pH_{pznpc}$ of ferrihydrite, indicating that the adsorption of arsenate also involves non-electrostatic (specific) interaction. This observed pH-dependent adsorption of arsenate also agrees with the calculated Gibbs free energy changes for the arsenate binding reaction with model ferric hydroxide. As shown in Figure 2, the Gibbs free energy ($\Delta G_r^0$) for arsenate binding reaction (binuclear bidentate complex was chosen as a representative surface complexation in the modeling) remains constant at pH < 7.0. The large negative value of the $\Delta G_r^0$ suggests the binding reaction is thermodynamically favorable under the pH conditions. At pH > 7.0, the Gibbs free energy of the reaction increases consistently with increasing pH, resulting in the decreased arsenate adsorption observed in the experimental data (Figure 1a).

The effect of $Si_{(aq)}$ on arsenate adsorption to ferrihydrite was examined in the dual metalloid systems containing 1.0 mM (28 mg $L^{-1}$) Si. This concentration was chosen because it represents that of Si in arsenic contaminated groundwater (Mariner et al., 1996). The presence of Si exhibits negligible effect on arsenate adsorption across the entire pH range regardless of the initial arsenate concentration (Figure 1a). This result agrees with prior work that showed negligible Si effect on arsenate adsorption to Fe oxides (Waltham and Eick, 2002; Roberts et al., 2004), suggesting that Si and arsenate are possibly adsorbed to different surface sites. Adsorption of Si was also measured as a function of pH in the dual metalloid systems. Adsorption was observed to increase with increasing pH to a maximum at pH 7 – 9, after which sorption decreased slightly with further increase in pH (Figure 1c). The pH-dependent adsorption can also be explained by the aqueous speciation of Si and surface charge of ferrihydrite. The first dissociation constant ($pKa_1$) of monomeric silicic acid is 9.8 (at 25 ºC), whereas the corresponding *p*Ka for oligomeric silicic acid is in the range of 9.5–10.7 (Makrides et al., 1980), indicating that silicic acid is present as a neutral species throughout most of the pH range of this study. Thus, adsorption is favored at pH values close to the pznpc of ferrihydrite, where the electrostatic repulsive force between adsorbent and adsorbate (and hence the Gibbs free energy for the binding reaction, Figure 2), are minimized. In addition, below the ferrihydrite pznpc, total Si uptake after 24 h was lower in the system containing higher arsenate concentration, suggesting that arsenate uptake diminishes Si adsorption to ferrihydrite surface (Figure 1c). The fact that arsenate can effectively displace silicic acid while silicic acid has negligible effects on arsenate adsorption can also be explained by the Gibbs free energies for the binding reactions of arsenate and silica on ferric hydroxide (Figure 2). Indeed, the greater extent of Si displacement occurs with decreasing pH where arsenate has much stronger binding energy than does silicic acid (Figures 1c & 2).

**3.1.2 Silicic acid effects on arsenite adsorption to ferrihydrite—**The results of batch adsorption of arsenite to ferrihydrite are shown in Figure 1b. Less than 5% of total arsenite was oxidized to arsenate during the experiments (data not shown), indicating that the preservation techniques were effective to minimize oxidation. The pH trend of arsenite

adsorption differs from arsenate (Figure 1b). Similar to Si, maximum arsenite adsorption to ferrihydrite occurs at pH close to the pznpc of ferrihydrite, as arsenious acid ($H_3AsO_3$) has similar *p*Ka values to silicic acid (Raven et al., 1998). The trend is less distinct at lower As surface loading (i.e., 0.1 mM), presumably due to the presence of excess mineral surface sites (Figure 1b).

In contrast to the case for arsenate, arsenite is subject to diminished adsorption as a result of competition from silicic acid. Although the amount of adsorbed arsenite decreased slightly when Si was present (Figure 1b), this translated to a significant (several-fold, depending on pH) increase in aqueous arsenite concentration at equilibrium (Figure S4). Hence, the presence of aqueous Si, at representative environmental concentrations, can be expected to increase significantly arsenic mobility and bioavailability in natural sub-oxic environments, as also suggested in some prior studies (Roberts et al., 2004; Luxton et al., 2006). Interestingly, the effect appears to be more pronounced at low (pH < ~6.0) and high pH ends (pH > 9.0) (Figures 1b and S4). The equilibrium aqueous concentration of arsenite after adsorption increased as much as nine times at low pH and three times at high pH when Si was present (Figure S4). The pronounced effect at high pH can be explained by a decrease in the isoelectric point (IEP) of ferrihydrite upon adsorption of $Si(OH)_4$. Prior studies have indicated that the adsorption of silicic acid to Fe oxyhydroxides decreases the IEP of the mineral sorbent, creating a stronger electrostatic repulsive force for adsorption of negatively charged oxyanions at pH above the IEP (Garman et al., 2004; Luxton et al., 2006). Mechanisms responsible for substantial reduction of arsenite adsorption at pH < 6.0 are more complex, and may involve multiple effects (e.g., ferrihydrite dissolution, surface site competition, surface-induced Si polymerization) that cannot be unambiguously determined from macroscopic batch adsorption results alone.

Adsorption of Si to ferrihydrite in the presence of arsenite exhibits similar pH-dependent trend to the system containing arsenate; adsorption increases with increasing pH to the sorption maximum and then decreases slightly with further increases in pH (Figure 1d), consistent with the Gibbs free energy changes for the binding reaction (Figure 2). The fact that lower Si adsorption (at pH < 6.0) was measured when arsenite was present at higher concentration can be attributed to surface site competition between the two neutral species $H_3AsO_3{}^0{}_{(aq)}$ and $Si(OH)_4{}^0{}_{(aq)}$.

### 3.2 ATR-FTIR spectroscopy

The spectra of aqueous arsenate species collected on the Ge IRE (without ferrihydrite film) as a function of pH were used as a basis to determine the surface complexes formed between arsenate and ferrihydrite (Figure 3a). These spectra are in good agreement with prior studies (Myneni et al., 1998; Roddick-Lanzilotta et al., 2002; Goldberg and Johnston, 2002). Briefly, at pH 3.0 and 6.0 ($pKa_1$ < pH < $pKa_2$ of arsenic acid) (Raven et al., 1998), arsenate is partially deprotonated and the $H_2AsO_4{}^-{}_{(aq)}$ species predominates, exhibiting a $C_{2v}$ symmetry. The bands at 907 and 877 $cm^{-1}$ correspond to the asymmetric and symmetric stretching of the two As-$O^-$ bonds, whereas the two bonds from As to protonated oxygens (As-OH) do not generate distinct IR bands in the spectral region (Figure 3a). With pH increase to 9.0 ($pKa_2$ < pH < $pKa_3$), arsenate dissociates its second proton, $HAsO_4{}^{2-}{}_{(aq)}$

predominates, and its symmetry changes from $C_{2v}$ to $C_{3v}$ (Figure 4). Consequently, the pH 9 spectrum differs significantly from those at lower pH, and exhibits a broad band at 857 $cm^{-1}$ corresponding to the asymmetric stretching of the As-O bonds, which is large and broad enough to also mask the symmetric stretching band.

The spectra of ferrihydrite-adsorbed arsenate species at the same pH values (3.0, 6.0 and 9.0) are shown in Figure 3b. The shoulder band at ~ 830 $cm^{-1}$ in spectra collected at pH 3.0 and 6.0 is attributed to the stretching vibration of As-O coordinating to the Fe metal center (i.e, As-O-Fe bond), whereas the band at *ca*. 884 $cm^{-1}$ results from non-surface-complexed As-O bonds of the adsorbed arsenate species (Goldberg and Johnston, 2002; Jia et al., 2007). The result is consistent with previous spectroscopic studies of arsenate adsorption on metal oxides, indicating the formation of *bidentate binuclear* inner-sphere complexes between arsenate and ferrihydrite surface hydroxyls (Goldberg and Johnston, 2002; Jia et al., 2007). With pH increasing to 9.0, the two stretching bands are shifted to lower wavenumber from 884 and 830 to 860 to ~ 804 $cm^{-1}$, respectively, indicting local changes in arsenate coordination chemistry, also consistent with prior work (Goldberg and Johnston, 2002; Roddick-Lanzilotta et al., 2002; Jia et al.; 2007). As indicated schematically (Figure 4), two possible binuclear bidentate complexes may form at ferrihydrite surfaces for arsenate species, distinguished on the basis of uncomplexed oxygen protonation state (protonated structure *a* or unprotonated structure *b*). We expect that arsenate forms adsorbed structure *a* at low pH where adsorbed arsenate is protonated, and structure *b* at higher pH where arsenate species are dissociated. Such structure changes are consistent with the pH-dependent shifts in As-O stretching bands observed in the spectra upon adsorption to ferrihydrite.

Arsenate spectra show negligible changes in response to $Si(OH)_{4(aq)}$ introduction irrespective of pH; no detectable peak shifts or emergence of new peaks were observed (Figure 3b and 3c), suggesting that the complexation mode of adsorbed arsenate was not affected by Si adsorption. These results are consistent with the negligible effect of Si on arsenate surface excess as indicated by batch adsorption data (Figure 1a). ATR-FTIR data also indicate that silica is adsorbed predominantly as monomeric silicate via bidentate linkage in the first hour of the sorption reaction, as indicated by the band at 945 $cm^{-1}$ (Figure 3d) (Swedlund et al., 2009; 2010), but that the spectra gradually change during the first 2 h of reaction time to exhibit a dominant band at ~1021 $cm^{-1}$ with a shoulder at ~1103 $cm^{-1}$ (Figure 3d). These latter bands correspond to discrete oligomeric silicate and polymeric silicate species, respectively (Swedlund et al., 2009). Therefore, the ATR-FTIR data reveal that Si is mainly retained at the ferrihydrite surface via interfacial polymerization reaction that occurs at the equilibrium Si concentration of 1.0 mM maintained in the flow-through system. It is important to note that the equilibrium $Si_{(aq)}$ concentration in the batch adsorption experiment was much lower than the initial concentration (i.e., 1.0 mM) because of ferrihydrite surface uptake from solution. Thus, surface-induced Si polymers observed in the ATR-FTIR results may not have been formed in the batch systems due to the relatively lower $Si_{(aq)}$ concentration.

### 3.3 Arsenic X-ray absorption spectroscopy (XAS)

Arsenic K-edge XAS spectroscopy was used to complement the ATR-FTIR data in determining the local coordination and bonding mechanisms of arsenate and arsenite adsorbed to ferrihydrite. Figure 5 shows (a) the XANES, (b) $\kappa^3$ weighted EXAFS, and (c) the corresponding Fourier transform (FT) results for the As(V)-adsorbed ferrihydrite samples. The structural parameters obtained from the non-linear least-squares fits of the EXAFS data are summarized in Table 1. The interatomic distance of the As-O shell (1.69 Å) and coordination number (CN) of 4 indicate that arsenate is present as $AsO_4$ tetrahedra in all samples (Waychunas et al. 1993, Farquhar et al., 2002). In addition to the major As-O shell, the additional small peak at 3.03 Å is due to a multiple scattering path from As-O-O in arsenate tetrahedra. No As-Fe backscattering at <3 Å was detected, and the FT peak beyond the MS feature can be attributed to As-Fe bonding at 3.27 Å. This bonding distance is in good agreement with a bidentate binuclear As-Fe bond previously reported for As(V) adsorbed to Fe oxyhydroxides (Manceau, 1995; Fendorf et al., 1997; Sherman and Randall, 2003; Arai et al., 2004; Beak et al., 2006; reviewed in Wang and Mulligan, 2008). Thus, the EXAFS results are consistent with the ATR-FTIR results, both suggesting that As(V) is predominantly adsorbed to ferrihydrite surfaces via bidentate binuclear, inner-sphere complexes. It should be mentioned that the spectroscopic data cannot rule out contributions to adsorption from outer-sphere complexation (i.e., electrostatic interaction) (Voegelin and Hug, 2003; Catalano et al., 2008). The differences detected by the ATR-FTIR spectroscopy between the low and high pH samples for arsenate adsorbed to ferrihydrite (Figure 3), presumably due to the presence of two types of bidentate binuclear complexes distinguished on the basis of protonation state (Figure 4), were not observed in the EXAFS data. The EXAFS spectra exhibit identical bond distance for the As-O bonds at pH 3.0 and 9.0 (Table 1), suggesting that protonation has negligible effects on interatomic distance of the As-O bonds in the $AsO_4$ tetrahedron as measured by EXAFS.

The EXAFS data also indicate that the presence of Si has negligible effects on As-Fe bonding mechanisms, which is consistent with the batch sorption and ATR-FTIR data. As indicated by the ATR-FTIR and EXAFS data, arsenate is bound to Fe-metal center via bidentate binuclear complexes. The determined CN for As-Fe bonds is close to the expected 2 for $^2$C bidentate binuclear complex, ranging from (1.3 to 2.1). The backscattering amplitude of the second shell As-Fe is greater in the samples with Si (1.8–2.1) than those without Si (1.3–1.5). The presence of Si apparently increases the As-Fe CN (Table 1), suggesting that in the absence of Si, arsenate was not as positionally ordered on the ferrihydrite surface or arsenate occupied some outer-sphere sites that are not probed with EXAFS.

On the basis of the fit for arsenite adsorbed to ferrihydrite, the As(III)-O bond distance was calculated to be 1.77–1.78 Å (Figure 6 and Table 1). The bond distances and CN (~3.3–3.4) from this study agree with other XAS investigations, and are indicative of the $AsO_3$ trigonal pyramidal structure (Waychunas et al., 1993; Farquhar et al., 2002). The bond distance, coordination geometry, and the absorption edge in the XANES spectra (Figure 6a) all suggest that oxidation of As(III) to As(V) did not occur during the reaction process, consistent with the results of the HPLC-ICP-MS arsenic speciation analysis. In addition to

the major As-O shell, two As-Fe bonds with respective interatomic distances of ~2.92–2.94 Å and ~3.41–3.44 Å were observed in the FT spectra, suggesting the presence of mixed As(III) bonding environments on the ferrihydrite surface. The bond distances are in good agreement with other prior EXAFS studies, and are indicative of both bidentate mononuclear complexation (i.e., AsFe $^{2}$E, edge sharing) and bidentate binuclear complexation with corner-sharing between $AsO_3$ pyramids and $FeO_6$ octahedral (i.e., AsFe $^{2}$C, corner sharing), respectively (Farquhar et al., 2002; Ona-Nguema et al. 2005; Root et al., 2007). No detectable changes were observed in the EXAFS spectra with pH increase from ~3.0 to ~9.0, indicating that the As(III)-Fe bonding mechanisms were unaffected by pH. The As(III) spectra were fit best with 2 As-Fe backscattering paths corresponding to $^{2}$E and $^{2}$C coordination. The short $^{2}$E distance at 2.93±0.01 Å is distinctly observed, and the longer distance is best fit to 3.42±0.02 Å. Fitting a third backscattering monodentate $^{1}$V shell at >3.5 Å did not significantly improve nor degrade the fit, as measured in the $\chi^2$ value, and cannot be ruled out. However, the backscattering amplitude for AsFe in $^{2}$E and $^{2}$C coordination were similar, and about twice the amplitude of a $^{1}$V distance when it was included.

The EXAFS spectra show similar bond distances for As(III)-Fe bonds in both the presence and absence of Si (Table 1), suggesting that competitive adsorption of $Si(OH)_{4(aq)}$ has insignificant effects on As(III)-Fe bonding modes. However, it is noteworthy that the average CN for As-Fe bonds significantly increased for samples at pH ~3.0 and 9.0, coincident with the pH values that showed the greatest competitive effect of Si that resulted in desorption of arsenite at low and high pH in the batch adsorption results (Figure 1b). This may reflect retention of arsenite at ferrihydrite surface binding sites of more stable coordination and desorption at sites where inner-sphere coordination is less stable, the latter being more susceptible to arsenite dissociation because of silicic acid competition.

### 3.4 Quantum DFT calculations

The Gibbs free energy changes for the formation of mono- and bidentate surface complexes of As(V), As(III) and $Si(OH)_4$ at the corner and edge sites of the ferric hydroxide cluster were calculated using DFT. The standard Gibbs energy change, the Gibbs energy change at pH 7 as well as the corresponding As-Fe bond distance are summarized in Table 2. The schematic diagram of each individual complex is also shown in Figure 10. In contrast to the molecular spectroscopic techniques (ATR-FTIR and EXAFS), the DFT model allows us to differentiate two monodentate surface coordinations (apical $^{a1}$V vs. equatorial $^{e1}$V) based on their Gibbs free energies of the binding reactions. Therefore, the DFT model was able to calculate the Gibbs free energies and As-Fe bond distances for four surface complexes. As shown in Table 2, the DFT model suggests that bidentate binuclear (corner sharing, As$^{V}$Fe $^{2}$C) complex (Figure 7) is the most thermodynamically favorable binding for arsenate adsorption on ferric hydroxide, consistent with the results of the ATR-FTIR and EXAFS data. The calculated interatomic bond distance of the As(V)-Fe bond is very close to the bond distance from the EXAFS data.

The DFT model predicted that arsenite should form equatorial-vertex sharing monodentate ($^{e1}$V) complexes on ferric hydroxide surface as suggested by the large negative Gibbs free

energies (Table 2 and Figure 10). While the preference of an arsenite-ferrihydrite $^{1}V$ complex is not consistent with the EXAFS results, the AsFe $^{e1}V$, $^{2}C$, and $^{2}E$ complexes all have large negative values for $\Delta G_r^0$ that range from −25.3($^{2}E$) to −32.6($^{e1}V$). Including the $^{1}V$ backscattering path in the EXAFS did not improve the fit in the spectra; however, a $^{1}V$ complex at the modeled distance of 3.32 Å could be masked by the other AsFe scattering paths. The calculated As(III) bond distances are substantially lower than bond distances observed by this and other EXAFS studies (Fendorf et al., 1997; Farquhar et al., 2002; Ona-Nguema et al., 2005; Root et al., 2007).

In addition, the DFT model predicted that arsenate is predominantly adsorbed to the ferric hydroxide surface at the corner sites, while both the corner and edge sites play important roles in arsenite adsorption (Table 2). The edge site binding of $Si(OH)_4$ is likely to compete with arsenite adsorption and have less effect on the corner binding of arsenate adsorption. This result provides a molecular-scale explanation for the greater susceptibility of arsenite, relative to arsenate, to desorb in the presence silicic acid (i.e., the locus of desorption being edge sites), and is in good agreement with the batch adsorption observations.

## 4. Conclusions

Conjunctive use of batch adsorption, ATR-FTIR and EXAFS spectroscopies, and DFT modeling enabled an improved understanding of As(V) and As(III) surface complexation at the ferrihydrite surface as affected by the competitive effects of silicic acid. The presence of dissolved silica at environmentally-relevant concentrations significantly decreased arsenite adsorption at low and high pH, whereas arsenate adsorption showed negligible response to elevated Si under the experimental conditions employed. This finding is inconsistent with a few previous batch sorption studies (Meng et al., 2000; Davis et al., 2001) which suggested that arsenate removal was substantially diminished by the presence of Si. This is most likely due to the concentration effect. The Si/As concentration ratio employed in this study is either 1 or 10, whereas the ratio is much higher (100–>1000) in those studies, resulting in desorption of arsenate from the sorbent surfaces. Indeed, Meng et al. (2000) reported that Si exhibits negligible effect on arsenate removal at low Si concentration, but significant impact at higher Si concentration. ATR-FTIR and EXAFS spectroscopies, as well as DFT calculations were internally consistent, with each showing the predominance of binuclear bidentate complexation for arsenate and both binuclear and mononuclear bidentate complexation for arsenite. Whereas ferrihydrite surface coordination of As(III) and As(V) species was unaffected by the presence versus absence of silicic acid, the greater susceptibility of arsenite (relative to arsenate) to desorption in the presence of dissolved Si is consistent with preferential, Si-induced, dissociation of arsenite at edge sites of ferrihydrite Fe octahedra.

## Supplementary Material

Refer to Web version on PubMed Central for supplementary material.

## Acknowledgments

This research was supported by the National Institute for Environmental Health Sciences, NIEHS SRP Grant 2 P42 ES04940. The authors thank Mary Kay Amistadi for total metal and As speciation analysis. Portions of this research were carried out at Stanford Synchrotron Radiation Laboratory, a National User Facility operated by Stanford University on behalf of the U.S. Department of Energy, Office of Basic Energy Sciences.

## References

Arai Y, Sparks DL, Davis JA. Effects of dissolved carbonate on arsenate adsorption and surface speciation at the hematite-water interface. Environ Sci Technol. 2004; 38:817–824. [PubMed: 14968869]

Beak DG, Basta NT, Scheckel KG, Traina SJ. Bioaccessibility of arsenic(V) bound to ferrihydrite using a simulated gastrointestinal system. Environ Sci Technol. 2006; 40:1364–1370. [PubMed: 16572798]

Beaulieu BT, Savage KS. Arsenate adsorption structures on aluminum oxide and phyllosilicate mineral surfaces in smelter-impacted soils. Environ Sci Technol. 2005; 39:3571–3579. [PubMed: 15952360]

Bednar AJ, Garbarino JR, Ranville JF, Wildeman TR. Preserving the distribution of inorganic arsenic species in groundwater and acid mine drainage samples. Environ Sci Technol. 2002; 36:2213–2218. [PubMed: 12038832]

Burleson DJ, Penn RL. Two-step growth of goethite from ferrihydrite. Langmuir. 2006; 22:402–409. [PubMed: 16378452]

Catalano JG, Park C, Fenter P, Zhang Z. Simultaneous inner- and outer-sphere arsenate adsorption on corundum and hematite. Geochim Cosmochim Acta. 2008; 59:3647–3653.

Davis CC, Knocke WR, Edwards M. Implications of aqueous silica sorption to iron hydroxide: Mobilization of iron colloids and interference with sorption of arsenate and humic substances. Environ Sci Technol. 2001; 35:3158–3162. [PubMed: 11505993]

Delley B. An all-electron numerical-method for solving the local density functional for polyatomic-molecules. J Chem Phys. 1990; 92:508–517.

Delley B. Fast calculation of electrostatics in crystals and large molecules. J Phys Chem. 1996; 100:6107–6110.

Delley B. From molecules to solids with the $DMol^3$ Approach. J Chem Phys. 2000; 113:7756–7764.

Delley B. The conductor-like screening model for polymers and surfaces. Mol Simulat. 2006; 32:117–123.

Dixit S, Hering JG. Comparison of arsenic(V) and arsenic(III) sorption onto iron oxide minerals: Implications for arsenic mobility. Environ Sci Technol. 2003; 37:4182–4189. [PubMed: 14524451]

Doelsch E, Masion A, Rose J, Stone WEE, Bottero JY, Bertsch PM. Chemistry and structure of colloids obtained by hydrolysis of Fe(III) in the presence of $SiO_4$ ligands. Colloids Surf A. 2003; 217:121–128.

Farquhar ML, Charnock JM, Livens FR, Vaughan DJ. Mechanisms of arsenic uptake from aqueous solution by interaction with goethite, lepidocrocite, mackinawite, and pyrite: An X-ray absorption spectroscopy study. Environ Sci Technol. 2002; 36:1757–1762. [PubMed: 11993874]

Fendorf S, Eick MJ, Grossl P, Sparks DL. Arsenate and chromate retention mechanisms on goethite. 1 Surface structure. Environ Sci Technol. 1997; 31:315–320.

Frau F, Biddau R, Fanfani L. Effect of major anions on arsenate desorption from ferrihydrite-bearing natural samples. Appl Geochem. 2008; 23:1451–1466.

Garman SM, Luxton TP, Eick MJ. Kinetics of chromate adsorption on goethite in the presence of sorbed silicic acid. J Environ Qual. 2004; 33:1703–1708. [PubMed: 15356230]

George, GN.; Pickering, IJ. EXAFSPAK: a suite of computer programs for analysis of X-ray absorption spectra. Stanford Synchrotron Radiation Laboratory; 2000.

Goh KH, Lim TT. Arsenic fractionation in a fine soil fraction and influence of various anions on its mobility in the subsurface environment. Appl Geochem. 2005; 20:229–239.

Goldberg S, Johnston CT. Mechanisms of arsenic adsorption on amorphous oxides evaluated using macroscopic measurements, vibrational spectroscopy, and surface complexation modeling. J Colloid Interface Sci. 2001; 234:204–216. [PubMed: 11161507]

Iler, RK. The Chemistry of Silica - Solubility, Polymerization, Colloid and Surface Properties, and Biochemistry. Wiley; New York: 1979.

Impellitteri CA. Effects of pH and phosphate on metal distribution with emphasis on As speciation and mobilization in soils from a lead smelting site. Sci Total Environ. 2005; 345:175–190. [PubMed: 15919538]

Jia YF, Xu LY, Wang X, Demopoulos GP. Infrared spectroscopic and X-ray diffraction characterization of the nature of adsorbed arsenate on ferrihydrite. Geochim Cosmochim Acta. 2007; 71:1643–1654.

Kelly CP, Cramer CJ, Truhlar DG. Adding explicit solvent molecules to continuum solvent calculations for the calculation of aqueous acid dissociation constants. J Phys Chem A. 2006; 110:2493–2499. [PubMed: 16480309]

Kubicki JD, Kwon KD, Paul KW, Sparks DL. Surface complex structures modelled with quantum chemical calculations: carbonate, phosphate, sulphate, arsenate and arsenite. Eur J Soil Sci. 2007; 58:932–944.

Liu F, De Cristofaro A, Violante A. Effect of pH, phosphate and oxalate on the adsorption/desorption of arsenate on/from goethite. Soil Sci. 2001; 166:197–208.

Luxton TP, Tadanier CJ, Eick MJ. Mobilization of arsenite by competitive interaction with silicic acid. Soil Sci Soc Am J. 2006; 70:204–214.

Makrides AC, Turner M, Slaughter J. Condensation of silica from supersaturated silicic acid solutions. J Colloid Interface Sci. 1980; 73:345–367.

Manceau A. The mechanism of anion adsorption on iron oxides: Evidence for the bonding of arsenate tetrahedra on free $Fe(O,OH)_6$ edges. Geochim Cosmochim Acta. 1995; 59:3647–3653.

Mariner PE, Holzmer FJ, Jackson RE, Meinardus HW, Wolf FG. Effects of high pH on arsenic mobility in a shallow sandy aquifer and on aquifer permeability along the adjacent shoreline, Commencement Bay Superfund Site, Tacoma, Washington. Environ Sci Technol. 1996; 30:1645–1651.

Meng XG, Bang S, Korfiatis GP. Effects of silicate, sulfate, and carbonate on arsenic removal by ferric chloride. Water Res. 2000; 34:1255–1261.

Mohan D, Pittman CU. Arsenic removal from water/wastewater using adsorbents - A critical review. J Haz Mat. 2007; 142:1–53.

Myneni SCB, Traina SJ, Waychunas GA, Logan TJ. Experimental and theoretical vibrational spectroscopic evaluation of arsenate coordination in aqueous solutions, solids, and at mineral-water interfaces. Geochim Cosmochim Acta. 1998; 62:3285–3300.

O'Day PA, Vlassopoulos D, Root R, Rivera N. The influence of sulfur and iron on dissolved arsenic concentrations in the shallow subsurface under changing redox conditions. P Natl Acad Sci USA. 2004a; 101:13703–13708.

O'Day PA, Rivera N, Root R, Carroll SA. X-ray absorption spectroscopic study of Fe reference compounds for the analysis of natural sediments. Am Mineral. 2004b; 89:572–585.

Ona-Nguema G, Morin G, Juillot F, Calas G, Brown GE. EXAFS analysis of arsenite adsorption onto two-line ferrihydrite, hematite, goethite, and lepidocrocite. Environ Sci Technol. 2005; 39:9147–9155. [PubMed: 16382936]

Paul KW, Kubicki JD, Sparks DL. Quantum chemical calculations of sulfate adsorption at the Al- and Fe- (hydr)oxide-$H_2O$ interfaces estimation of Gibbs free energies. Environ Sci Technol. 2006; 40:7717–7724. [PubMed: 17256518]

Raven KP, Jain A, Loeppert RH. Arsenite and arsenate adsorption on ferrihydrite: Kinetics, equilibrium, and adsorption envelopes. Environ Sci Technol. 1998; 32:344–349.

Rehr JJ. Recent developments in multiple-scattering calculations of XAFS and XANES. Jpn J Appl Phys. 1993; 32:8–12.

Roberts LC, Hug SJ, Ruettimann T, Billah M, Khan AW, Rahman MT. Arsenic removal with iron(II) and iron(III) waters with high silicate and phosphate concentrations. Environ Sci Technol. 2004; 38:307–315. [PubMed: 14740752]

Roddick-Lanzilotta AJ, McQuillan AJ, Craw D. Infrared spectroscopic characterization of arsenate (V) ion adsorption from mine waters, Macraes mine, New Zealand. Appl Geochem. 2002; 17:445–454.

Root RA, Dixit S, Campbell KM, Jew AD, Hering JG, O'Day PA. Arsenic sequestration by sorption processes in high-iron sediments. Geochim Cosmochim Acta. 2007; 71:5782–5803.

Ryu JH, Gao SD, Dahlgren RA, Zierenberg RA. Arsenic distribution, speciation and solubility in shallow groundwater of Owens Dry Lake, California. Geochim Cosmochim Acta. 2002; 66:2981–2994.

Schwertmann, U.; Cornell, RM. Iron Oxides in the Laboratory: Preparation and Characterization. Wiley-VCH; Weinheim, Germany: 1991.

Sherman DM, Randall SR. Surface complexation of arsenic (V) to iron(III) (hydr)oxides: Structural mechanism from ab initio molecular geometries and EXAFS spectroscopy. Geochim Cosmochim Acta. 2003; 67:4223–4230.

Sun XH, Doner HE. An investigation of arsenate and arsenite bonding structures on goethite by FTIR. Soil Sci. 1996; 161:865–872.

Swedlund PJ, Miskelly GM, McQuillan AJ. An attenuated total reflectance IR study of silicic acid adsorbed onto a ferric oxyhydroxide surface. Geochim Cosmochim Acta. 2009; 73:4199–4214.

Swedlund PJ, Miskelly GM, McQuillan AJ. Silicic acid adsorption and oligomerization at the ferrihydrite-water interface: Interpretation of ATR-IR spectra based on a model surface structure. Langmuir. 2010; 26:3394–3401. [PubMed: 20104911]

Voegelin A, Hug SJ. Catalyzed oxidation of arsenic As(III) by hydrogen peroxide on the surface of ferrihydrite: an in situ ATR-FTIR study. Environ Sci Technol. 2003; 37:972–978. [PubMed: 12666928]

Waltham CA, Eick MJ. Kinetic of arsenic adsorption on goethite in the presence of sorbed silicic acid. Soil Sci Soc Am J. 2002; 66:818–825.

Wang S, Mulligan CN. Speciation and surface structure of inorganic arsenic in solid phases: A review. Environ Int. 2008; 34:867–879. [PubMed: 18164403]

Waychunas GA, Rea BA, Fuller CC, Davis JA. Surface chemistry of ferrihydrite. Part 1: EXAFS studies of the geometry of coprecipitated and adsorbed arsenate. Geochim Cosmochim Acta. 1993; 57:2251–2269.

Webb, SM. SixPACK: Sam's Interface for XAS Package. Stanford Synchrotron Radiation Laboratory; 2006. http://www-ssrl.slac.stanford.edu/~swebb/

Yu JY, Heo B, Choi IK, Cho JP, Chang HW. Apparent solubilities of schwertmannite and ferrihydrite in natural stream waters polluted by mine drainage. Geochim Cosmochim Acta. 1999; 63:3407–3416.

Zhang N, Blowers P, Farrell J. Evaluation of density functional theory methods for studying chemisorption of arsenite on ferric hydroxides. Environ Sci Technol. 2005; 39:4816–4822. [PubMed: 16053079]

Zhu M, Paul KW, Kubicki JD, Sparks DL. Quantum chemical study of arsenic(III, V) adsorption on Mn-Oxides: Implications for arsenic(III) oxidation. Environ Sci Technol. 2009; 43:6655–6661. [PubMed: 19764231]

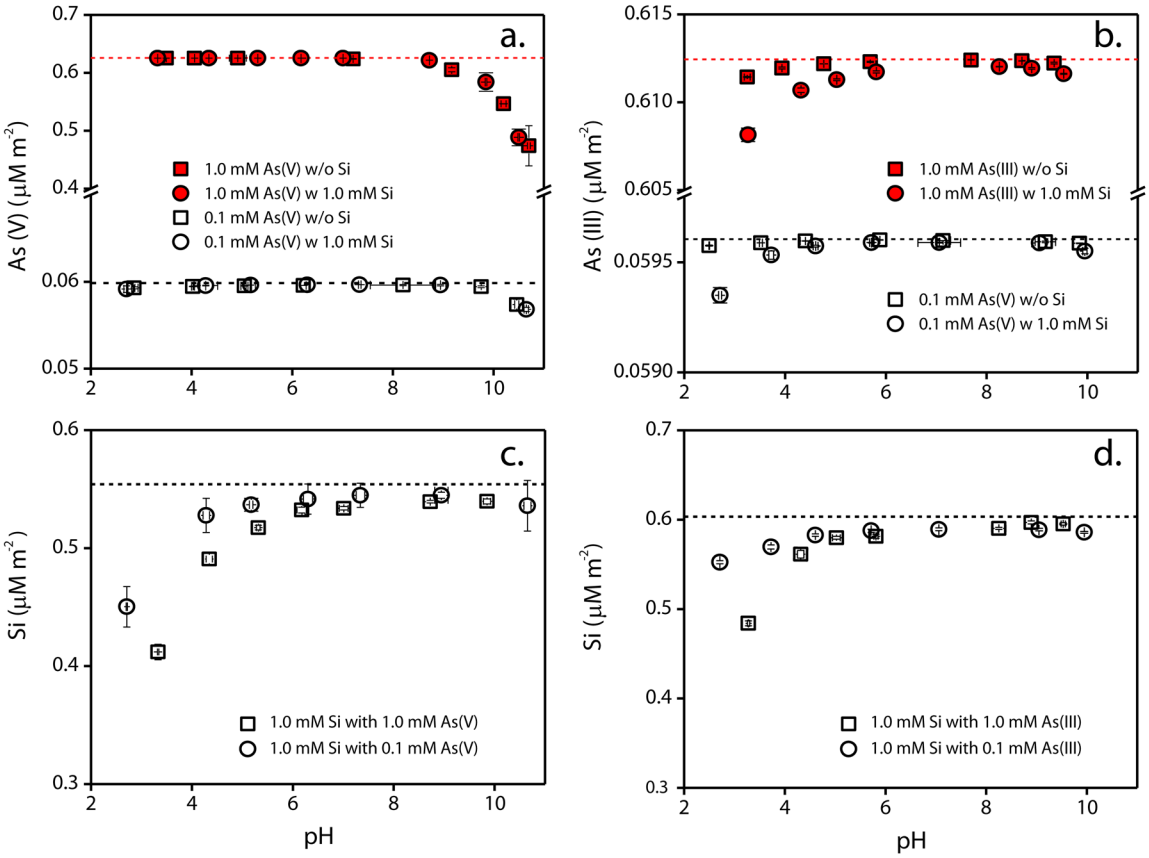


**Figure 1.**

(a) Arsenate and (c) arsenite adsorption on 6-L ferrihydrite in the absence or presence of 1.0 mM silicic acid as a function of pH; silicic acid adsorption on 6-L ferrihydrite in the presence of 0.1 or 1.0 mM arsenate (b) or arsenite (d) as a function of pH. The horizontal dash line represents 100% sorption

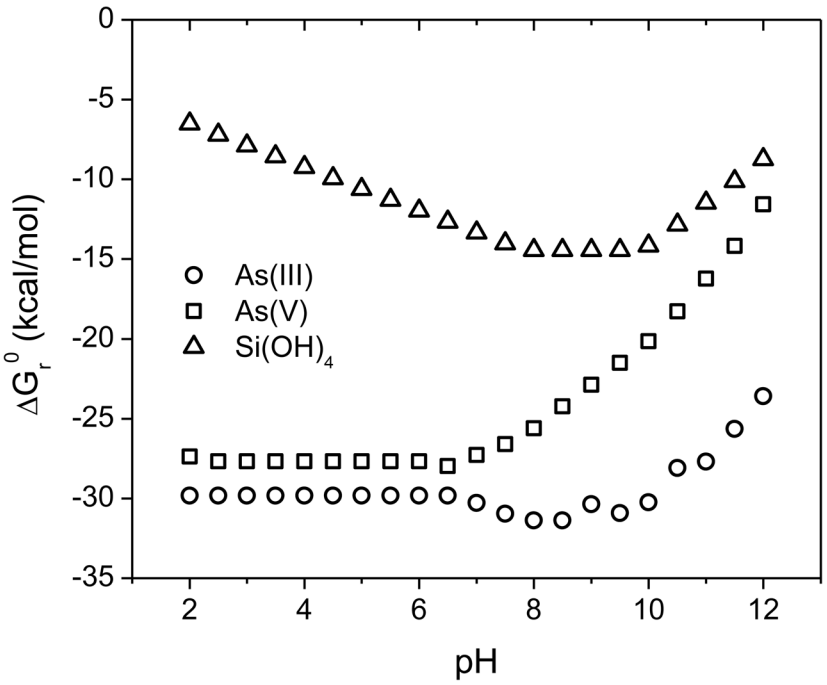


**Figure 2.**
Gibbs free energy changes for the bidentate binding reactions of As(III), As(V) and $Si(OsH)_4$ with ferric hydroxide as a function of pH.

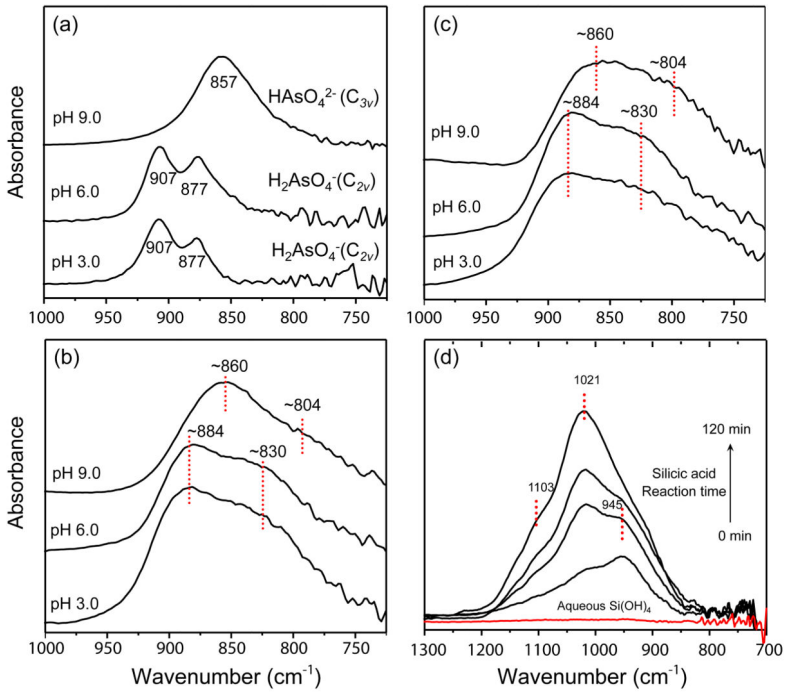


**Figure 3.**

ATR-FTIR spectra of 1.0 mM arsenate (V) adsorbed to (a) Ge IRE, (b) ferrihydrite in the absence of Si, and (c) ferrihydrite in the presence of 1.0 mM Si, as a function of pH; and (d) ATR-FTIR spectra of 1.0 mM silicic acid adsorbed to ferrihydrite as a function of reaction time at 0, 30, 60, 120 min. The spectrum of aqueous $Si(OH)_4$ was included for comparison.

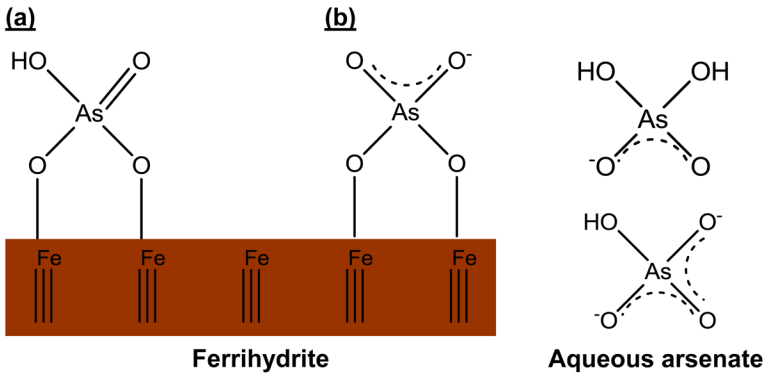


**Figure 4.**
Schematic diagram of As(V)-ferrihydrite complexes.

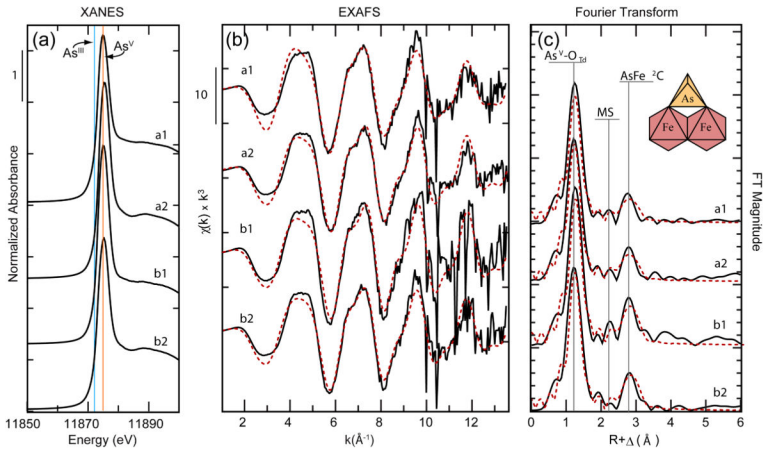


**Figure 5.**

Arsenic K-edge XANES, EXAFS, and Fourier transforms (FTs) of As(V)-adsorbed ferrihydrite samples in the absence of Si at pH 3.0 (a1) and 9.0 (a2) and in the presence of Si at pH 3.0 (b1) and 9.0 (b2).

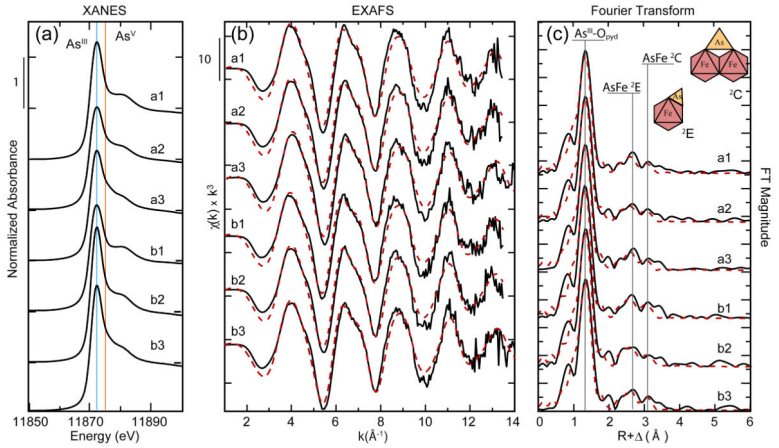


**Figure 6.**

Arsenic K-edge XANES, EXAFS, and Fourier transforms (FTs) of As(III)-adsorbed ferrihydrite samples in the absence of Si at pH 3.0 (a1), 6.0 (a2), and 9.0 (a3) and in the presence of Si at pH 3.0 (b1) 6.0 (b2), and 9.0 (b3).

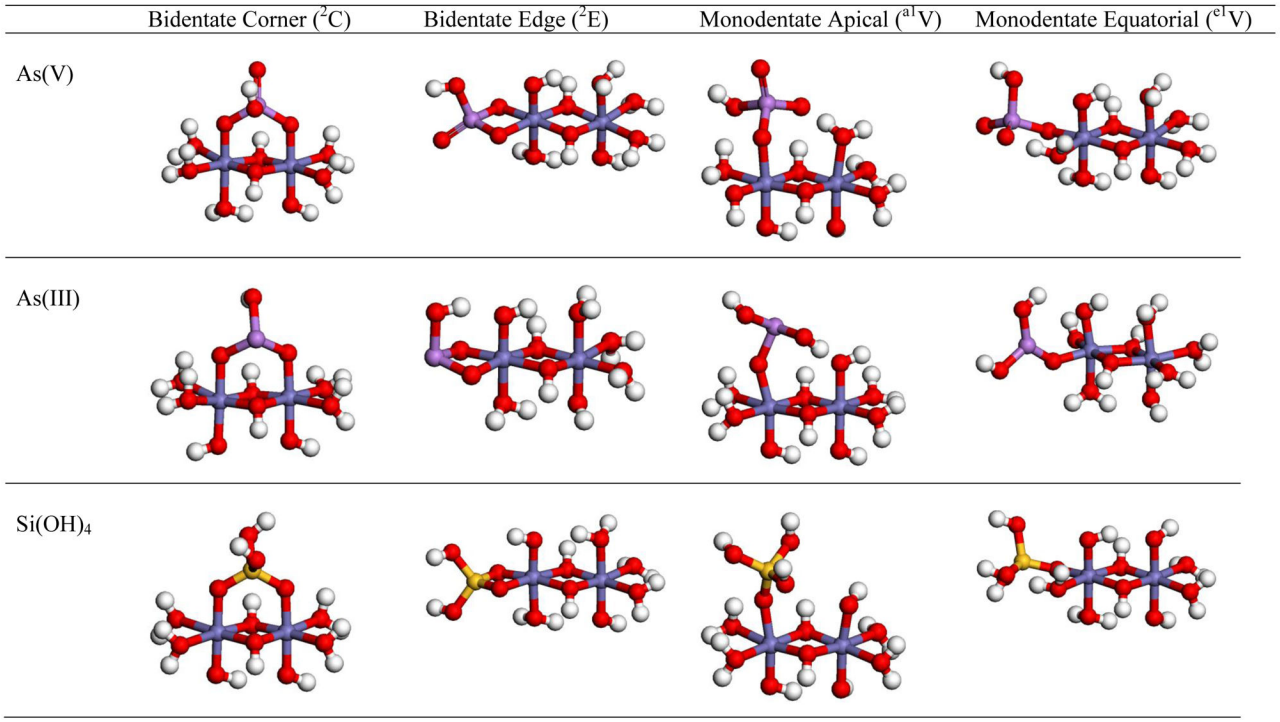


**Figure 7.**

Surface complexes of As(V), As(III) and $Si(OH)_4$ on ferric hydroxide. H = grey, O = red, Fe = blue, As(III) or As(V) = purple, Si = yellow.

**Table 1**

Arsenic K-edge EXAFS fit results

| Sample | Atom[a] | N | R (Å) | $\sigma^2$ (Å$^2$) | $\Delta E_0$ (eV) | $\chi^2$ |
|---|---|---|---|---|---|---|
| *As(V)* | | | | | | |
| As(V) alone pH 3.0 | O | 4.0[b] | 1.68 | 0.0029 | −5.79 | 3.99 |
| | MS[c] | 12.0[d] | 3.03[d] | 0.0042[d] | | |
| | Fe | 1.5 | 3.28 | 0.004[b] | | |
| As(V) alone pH 9.0 | O | 4.0[b] | 1.69 | 0.0029 | −6.70 | 3.68 |
| | MS[c] | 12.0[d] | 3.04[d] | 0.0042[d] | | |
| | Fe | 1.3 | 3.27 | 0.004[b] | | |
| As(V)/Si pH 3.0 | O | 4.0[b] | 1.68 | 0.0023 | −6.67 | 11.5 |
| | MS[c] | 12.0[d] | 3.03[d] | 0.0034[d] | | |
| | Fe | 2.1 | 3.28 | 0.004[b] | | |
| As(V)/Si pH 9.0 | O | 4.0[b] | 1.69 | 0.0029 | −5.20 | 3.94 |
| | MS[c] | 12.0[d] | 3.04[d] | 0.0042[d] | | |
| | Fe | 1.8 | 3.28 | 0.004[b] | | |
| *As(III)* | | | | | | |
| As(III) alone pH 3.0 | O | 3.39 | 1.77 | 0.004[b] | 1.03 | 0.74 |
| | Fe | 0.83 | 2.94 | 0.008[b] | | |
| | Fe | 0.85 | 3.43 | 0.008[b] | | |
| As(III) aloneph pH 6.0 | O | 3.39 | 1.78 | 0.004[b] | 1.33 | 0.75 |
| | Fe | 0.77 | 2.92 | 0.008[b] | | |
| | Fe | 0.97 | 3.42 | 0.008[b] | | |
| As(III) alone pH 9.0 | O | 3.34 | 1.77 | 0.004[b] | 2.18 | 0.68 |

| Sample | Atom[a] | N | R (Å) | $\sigma^2$ (Å$^2$) | $\Delta E_0$ (eV) | $\chi^2$ |
|---|---|---|---|---|---|---|
| | Fe | 0.80 | 2.93 | 0.008[b] | | |
| | Fe | 0.83 | 3.41 | 0.008[b] | | |
| As(III)/Si pH 3.0 | O | 3.35 | 1.78 | 0.004[b] | 1.14 | 0.85 |
| | Fe | 0.88 | 2.94 | 0.008[b] | | |
| | Fe | 1.07 | 3.44 | 0.008[b] | | |
| As(III)/Si pH 6.0 | O | 3.23 | 1.78 | 0.004[b] | 1.15 | 0.75 |
| | Fe | 0.89 | 2.92 | 0.008[b] | | |
| | Fe | 0.92 | 3.41 | 0.008[b] | | |
| As(III)/Si pH 9.0 | O | 3.38 | 1.77 | 0.004[b] | 1.93 | 0.76 |
| | Fe | 0.91 | 2.92 | 0.008[b] | | |
| | Fe | 1.02 | 3.42 | 0.008[b] | | |

[a] Atom is the As-near neighbor ligand (O, Fe); N is the number of backscattering atoms at distance (R); $\sigma^2$, the Debye-Waller term, is the absorber-backscatterer mean-square relative displacement; $\Delta E_0$ is the threshold energy difference; $\chi^2$ is a reduced least-squares goodness-of-fit parameter (=F-factor/(# of points − # of variables) and $F = [\Sigma k^6(\chi_{exptl}-\chi_{calcd})^2/\Sigma k^6\chi_{exptl}^2]^{1/2}$); Scale factor ($S_0^2$) = 1. The $\sigma^2$ term and N cannot be co-varied.

[b] Parameter fixed in least-squares fit using value from fits to reference compounds;

[c] spectrum fit with a multiple scattering path from As-O-O in arsenate tetrahedron;

[d] parameter linked in fit to the parameter directly above constrained by MS path.

**Table 2**

The standard Gibbs energy change ( $\Delta G^{\circ}_{rxn}$) and the Gibbs energy change at pH 7 ($\Delta G^{pH=7}$) for the formation of uncharged monodentate and bidentate surface complexes of As(V), As(III) and $Si(OH)_4$.

| | Species | Complex | Site | Symbol | As-Fe (Å) | $\Delta G^{\circ}_{rxn}$ | $\Delta G^{pH=7}$ |
|---|---|---|---|---|---|---|---|
| As(V) | **$H_2AsO_4^-$** | **bidentate** | **corner** | $^{2}C$ | 3.231 | **−19.7** | **−29.2** |
| | $H_2AsO_4^-$ | monodentate | apical | $^{a1}V$ | 3.360 | −6.6 | −16.1 |
| | $H_2AsO_4^-$ | bidentate | edge | $^{2}E$ | 2.720 | −7.36 | −16.9 |
| | $H_2AsO_4^-$ | monodentate | equatorial | $^{e1}V$ | 3.280 | +2.69 | −6.85 |
| As(III) | **$H_3AsO_3$** | **bidentate** | **corner** | $^{2}C$ | 3.200 | **−31.4** | **−31.4** |
| | $H_3AsO_3$ | monodentate | apical | $^{a1}V$ | 3.538 | −13.7 | −13.7 |
| | $H_3AsO_3$ | bidentate | edge | $^{2}E$ | 2.744 | −25.3 | −25.3 |
| | **$H_3AsO_3$** | **monodentate** | **equatorial** | $^{e1}V$ | 3.323 | **−32.6** | **−32.6** |
| $Si(OH)_4$ | $Si(OH)_4$ | bidentate | corner | $^{2}C$ | | −14.43 | −14.43 |
| | $Si(OH)_4$ | monodentate | apical | $^{a1}V$ | | −8.91 | 8.91 |
| | **$Si(OH)_4$** | **bidentate** | **edge** | $^{2}E$ | | **−21.6** | **−21.6** |
| | $Si(OH)_4$ | monodentate | equatorial | $^{e1}V$ | | −14.47 | −14.47 |